

Recent Developments on Lightweight, Flexible, Dual Polarization/Frequency Phased Arrays using RF MEMS Switches on LCP Multilayer Substrates for Remote Sensing of Precipitation

Ramanan Bairavasubramanian, Nickolas Kingsley, Gerald DeJean, Guoan Wang,
Dimitrios E. Anagnostou, Manos Tentzeris, and John Papapolymerou

Georgia Institute of Technology, School of Electrical and Computer Engineering,
85 Fifth Street, Technology Square Research Building,
Atlanta, GA-30308

Abstract—The development of a dual-frequency, dual polarization, aperture-fed, multiple-layered microstrip antenna array on flexible organic material for System-on-a-Package (SoP) RF front ends, is described in this work. The integration of RF MEMS phase shifters with the array enables accurate beamscanning over the Earth's surface. The flexible lightweight organic substrate minimizes the production cost while it enables the structure to be folded or rolled-up thus saving space and weight, elements determinant in a satellite mission.

Index Terms—Antenna, Array, MEMS, Liquid Crystal Polymer (LCP).

I. INTRODUCTION

THE global water cycle is critical for the functioning of the Earth's system, as it integrates the physical, chemical and biological processes that sustain ecosystems and influence climate, weather, natural hazards and related global changes. Water evaporation, precipitation and water vapor feedbacks alter the surface and atmospheric heating and cooling rates, which lead to adjustments in atmospheric circulation and precipitation patterns - processes that are not adequately taken into account by currently used climate models. Sufficient understanding of such phenomena and processes is a key source for accurate prediction of the planet's climate through the development of models that respond to the water cycle's variability and changes that take place. For these reasons, water cycle research is a high-priority area of research.

The major issue for all space missions is the minimization of equipment's weight and cost, including the antennas. To monitor precipitation patterns, NASA requires dual-frequency (14/35 GHz for rain and 19/37 GHz for snow), dual-polarization space radar and radiometers. Moreover, it is desirable that the systems simultaneously measure the precipitation over the same area, which implies that the antenna radiation pattern should be the same for both frequencies and polarizations.

High-gain parabolic reflectors used in most space missions are bulky, heavy, difficult to deploy, expensive and have a limited scanning capability. Moreover, limitations of current technology include low antenna efficiency, difficulty in maintaining the uniform membrane spacing and surface flatness, increased sidelobe levels and single-frequency operation.

While past efforts have developed deployable antenna structures, they have not been dual-frequency and dual polarization, and past antennas that met those goals were non-deployable or were based on large weight/volume and high cost technology. NASA's latest efforts in collaboration with the Georgia Institute of Technology are in the development of advanced, low-cost, low-mass, deployable antennas with large surface that can be rolled-up or folded for launch and then deployed in space. Electronic scanning and shaping of the radiation patterns of the two beams at the two frequencies is desirable in order to cover the same area simultaneously.

In this work, recent developments on a dual-frequency, dual-polarized antenna array on a flexible Liquid Crystal Polymer (LCP) organic substrate are presented. LCP can be processed up to 300°C, has excellent electrical properties, very low moisture absorption, can be utilized in multiple layers, and can be folded or rolled. Figure 1 shows how in this multi-layer substrate, the complete feed network is integrated with the dual-polarized microstrip patch antennas for each frequency band. Lastly, RF MEMS phase shifters and switches are integrated onto the feed network to control the RF signal path, to select between the two available polarizations and to permit wide beam scanning.

II. DEVELOPMENT OF DUAL FREQUENCY ANTENNA ARRAYS

A. Array Design

The substrate used in this work is LCP. Some of the advantages of this organic substrate include low dielectric loss ($\tan\delta \sim 0.004$), constant dielectric permittivity at the

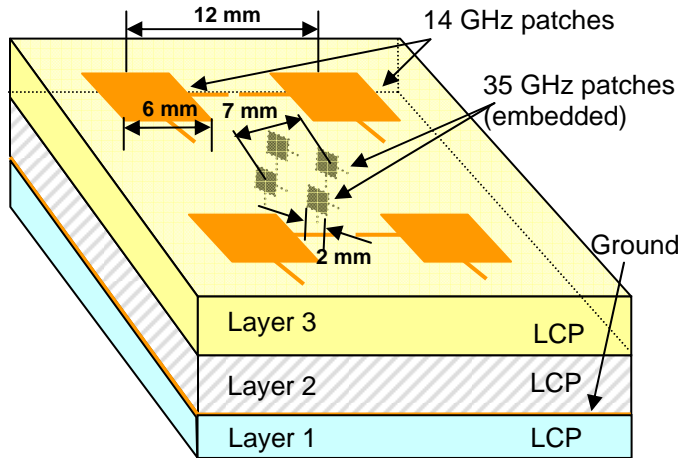


Fig. 1. Topology of the dual-frequency, dual-polarization flexible 2x2 antenna sub-array. The 35 GHz elements are embedded between the two LCP layers. The substrate layers have different color for illustrative purposes only. The dimensions of the structure are also shown.

frequencies of interest ($\epsilon_r \sim 3.15$), low moisture absorption ($<0.02\%$), light weight, mechanical stiffness, thermal stability (CTE = 0-30 ppm/ $^{\circ}\text{C}$), chemical resistance, ease of mass fabrication and great flexibility which allows for the material to be rolled up, which is ideal for circuits and structures that need to be deployed in space.

When designing dual-frequency, dual polarized microstrip antenna arrays, one has to confront many parameters of interest and the associated complexity both in design and fabrication. There is a need for a complex feeding structure that minimizes interconnect loss, feedline radiation and cross coupling. Substrate thickness can affect cross-polarization levels as well as bandwidth and efficiency. The distance of the antenna elements in the array can affect the -3 dB array beamwidth, its directivity and the side-lobe levels besides impacting the overall size. Careful consideration needs to be given to avoid cross coupling between the antenna arrays operating at different frequencies, blockage effects and edge diffraction. As a large amount of computational time is required to investigate the possibility of achieving all the aforementioned performance characteristics with a single layer structure, a multilayer architecture was utilized. Our multilayer structure can also result in very compact designs.

Figure 2 shows the side view and the top view (with all the layers interlaced) of the aperture coupled antenna array. The metal for the ground plane and the antenna elements is copper (Cu) and had a thickness of $18\mu\text{m}$. The total substrate thickness for this configuration is $457.2\mu\text{m}$ (18 mils). The radiating elements for both arrays are placed on one side of the ground plane, while the feed network for both arrays is placed on the other side. The ground plane itself contains slots through which energy is electromagnetically coupled from the feed network to the patches. The 35 GHz patches

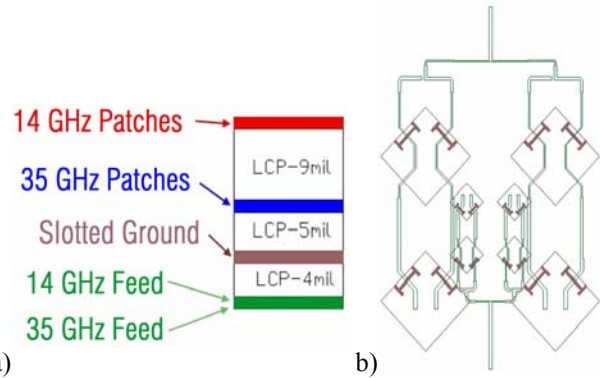


Fig. 2. a) Cross-section of the array layers, b) Final Array layout. All layers are visible so that the antennas, the slots and the feed network structure can be observed.

are placed on a $127\mu\text{m}$ (5 mils) thick LCP substrate, while the 14 GHz patches are placed on a $355.6\mu\text{m}$ (14 mils) thick LCP substrate. The feed network for both patches is placed on a $101.6\mu\text{m}$ (4 mils) thick LCP substrate on the other side. A combination of series and parallel feed was employed to form the 2x2 array. The 2x2 array is formed by a parallel combination of two linear 2x1 arrays, while the elements within a linear array are fed serially. Although many possibilities of substrate and feed configurations exist, this arrangement is chosen to meet three major requirements of this application:

- The return loss and radiation characteristics for both polarizations need to be identical.
- The return loss and radiation characteristics for both frequencies need to be similar.
- Polarization and beam steering requires integration of antenna arrays with MEMS and MEMS based phase shifters and attenuators.

To meet the first requirement, the radiating patches are rotated by 45° and the polarization directions are at 45° and 135° , while the array is still expanded in the traditional x-y direction. This allows the realization of a symmetrical feed structure with respect to two polarizations keeping the array characteristics identical between them. Appropriate substrate thickness and element spacing were chosen to meet the second requirement, while an aperture coupled feeding was chosen to meet the third requirement. The aperture coupled feeding not only reduces parasitic radiation from the feedlines but also allows placement of feed networks for both bands in the same layer. This, in turn, allows the placement of all the MEMS based devices in a single layer, thereby reducing fabrication complexity and packaging cost.

As this sub-array employs only canonical shapes, it can be cascaded in both longitudinal and transverse directions. A theoretical investigation illustrated that 12 sub-arrays of this type can provide a beamwidth smaller than 3° to a specific direction.

B. Fabrication

A critical step in the fabrication process is the bonding of the substrates, which is possible because of the availability of two types of LCP layers - low-melt (type-I LCP) bond layer and high-melt (type-II LCP) core layer. The bond layer melts at a lower temperature than the core layers and its flow coupled with the tool pressure applied between the core layers results in multilayer LCP structures. The cost of fabrication is low due to LCP's low processing cost, while low deployment costs result from the capability to roll/unroll the substrate and

thus the structure. The bonding process was optimized for temperature and tool pressure to prevent shrinkage, formation of bubbles, and melting of the core layers. For the multilayer antenna array structure, accurate alignment between different layers is necessary. This is facilitated by drilling precision alignment holes using a laser system. Three different laser systems, the CO_2 laser, the *Excimer* laser and the *infrared* laser, were used depending on the desired alignment accuracy levels. These holes were drilled before the individual layers were patterned. The alignment marks in the masks, which contain the patterns, were aligned to the laser holes drilled on the substrates during photolithography. After the individual substrates were patterned, alignment was maintained during bonding using alignment pins in the bonding press plates. This specific alignment procedure is unique and essential in creating multilayer antenna structures operating at mm-wave frequencies that require very precise alignment. Figure 3(a) shows the individual patterned layers of the aperture-fed array before bonding and Figure 3(b) shows the array after bonding.

C. Results

For measurement purposes, the dual-frequency array was excited at one frequency, while the other was treated as parasitic. The simulated and measured return loss results of the 14 GHz array are shown in Figure 4. The impedance characteristics are summarized in Table I. Figure 5 shows the return loss results for the 35 GHz array and Table II summarizes the impedance characteristics. The results show a frequency shift of 200 MHz for the 14 GHz and of 250 MHz for the 35 GHz array. The 14 GHz array's return loss is slightly smaller than the simulated, possibly due to mismatch at the input terminals between the connector and the feeding structure. The measured impedance bandwidths at both frequencies are in good agreement with the simulated. The 2-D radiation pattern results for the 14 GHz are shown in Figures 6(a,b). The radiation characteristics of the 14 GHz array are summarized in Table III. The 2D radiation pattern results for the 35 GHz are shown in Figures 7(a,b). The radiation characteristics of the 14 GHz array are summarized in Table IV. Again, the simulation and measured results agree very well. All the results shown are for one polarization, but

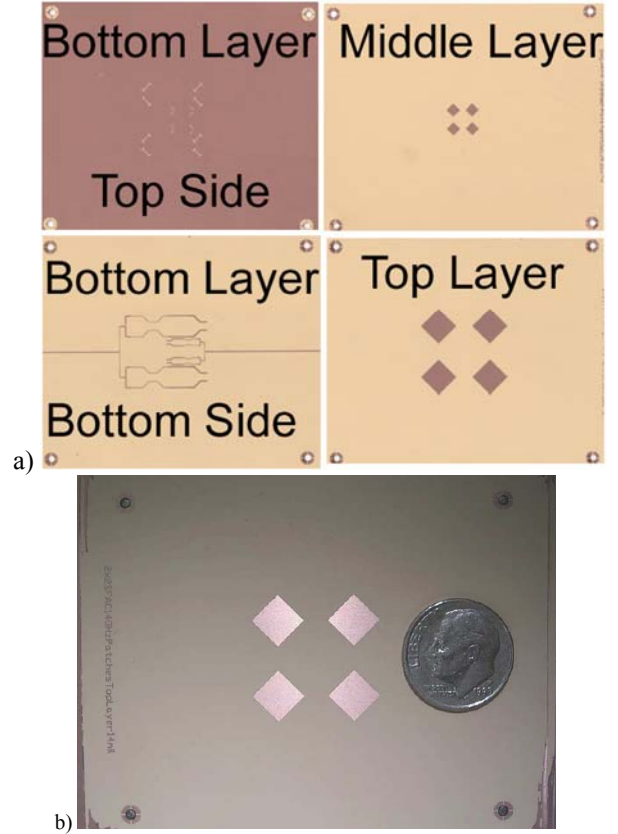


Fig. 3. Fabricated Images of the of the aperture-fed microstrip array: a) Photos of the individual patterned layers. b) Photo of the bonded array. Only the 14 GHz patches on the top layer are visible.

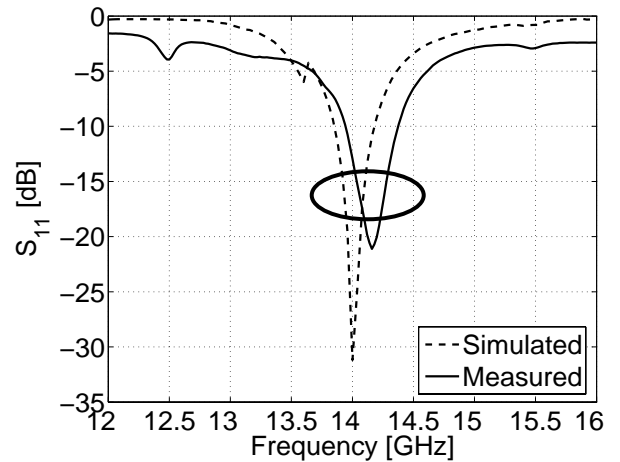


Fig. 4. Simulated and measured return loss of the array at 14 GHz.

TABLE I
RETURN LOSS CHARACTERISTICS OF THE 14 GHz ARRAY

Characteristic	Simul. 14 GHz	Measured 14 GHz
Resonant Frequency	14 GHz	13.72 GHz
Return Loss	30.7dB	20.6 dB
Bandwidth	140 MHz	160 MHz

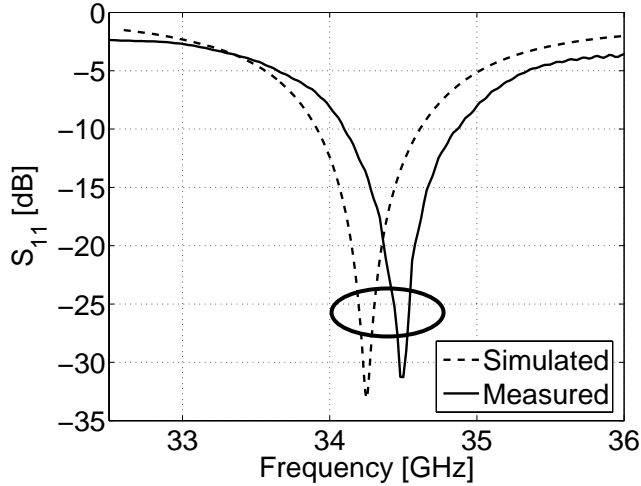


Fig. 5. Simulated and measured return loss of the array at 35 GHz.

TABLE II
RETURN LOSS CHARACTERISTICS OF THE 35 GHz ARRAY

Characteristic	Simul. 35 GHz	Measured 35 GHz
Resonant Frequency	34.87 GHz	34.32 GHz
Return Loss	32.5dB	31.1 dB
Bandwidth	1560 MHz	1530 MHz

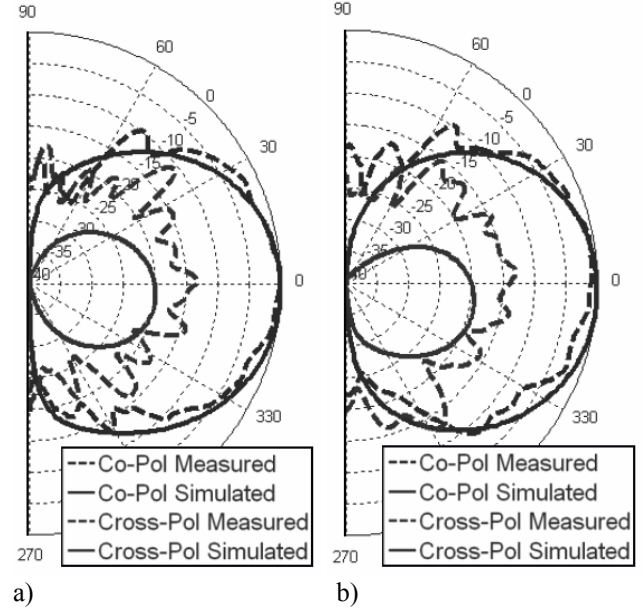


Fig. 7(a, b). a) E-plane radiation pattern of the 35 GHz array. b) H-plane radiation pattern of the 35 GHz array.

TABLE IV
RADIATION PATTERN CHARACTERISTICS OF THE 35 GHz ARRAY

Characteristic	Simul. 14 GHz	Measured 14 GHz
E-Plane $-\Theta_{bw}$ (-3 dB)	65°	66°
H-Plane $-\Theta_{bw}$ (-3 dB)	59°	59°
Max.E-plane cross-pol level	-15 dB	-13 dB
Max.H-plane cross-pol. level	-16 dB	-15 dB

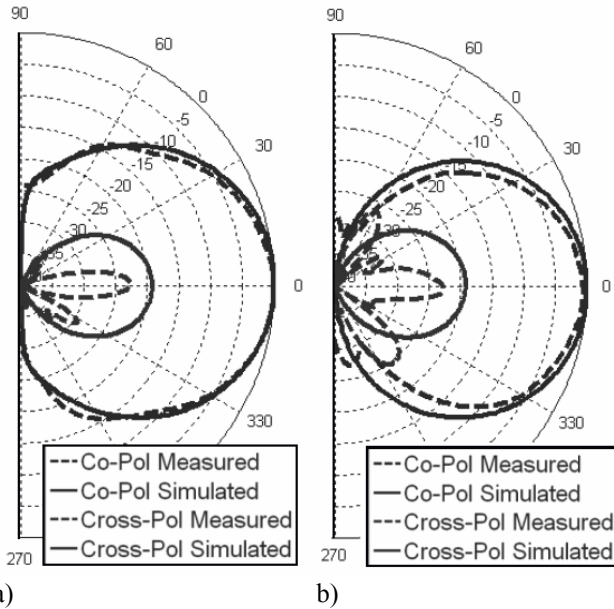


Fig. 6(a, b). a) E-plane radiation pattern of the 14 GHz array. b) H-plane radiation pattern of the 14 GHz array.

TABLE III
RADIATION PATTERN CHARACTERISTICS OF THE 14 GHz ARRAY

Characteristic	Simul. 14 GHz	Measured 14 GHz
E-Plane $-\Theta_{bw}$ (-3 dB)	65°	67°
H-Plane $-\Theta_{bw}$ (-3 dB)	58°	58°
Max.E-plane cross-pol. level	-31 dB	-16 dB
Max.H-plane cross-pol. level	-33 dB	-25 dB

they are the same for the other orthogonal polarization also due to the symmetric arrangement of radiating elements and the feed network. Thus, the designs can function as a dual frequency and dual polarization antenna array system. In order to realize a polarization reconfigurable system (i.e. to switch between polarizations in real-time), switches need to be integrated with the current arrays. This is discussed in the next section.

III. MONOLITHICALLY INTEGRATED RF MEMS SWITCH

Monolithically integrating MEMS devices on LCP initially improved to be a non-trivial task. Fabricating on a flexible, organic substrate is not as straightforward as using a smooth, flat substrate like silicon. Being a flexible material, it is prone to curling. This effect becomes more pronounced throughout processing due to the fluctuation of temperature from the various baking, deposition, and etching steps.

Since optical lithography with a 3-5 μm resolution cannot be performed on a curled substrate, it is necessary to mount the sample to a flat, clean room grade material before processing. Temporary mounting can be done using a spin-on or roll-on adhesive. Permanent mounting could also be used if a rigid substrate is desired. Since the substrate is also an

organic polymer, surface roughness is an issue. The surface roughness is usually on the order of 2-5 μm . Given that the MEMS switch is generally suspended 2-3 μm above the substrate, the surface roughness can be large enough to prevent the switch from deflecting. To solve this problem, each sample is mechanically polished using alumina slurry. After polishing, the sample will have a surface roughness between 10-50 nm, which is smooth enough for MEMS switch operation [3].

After polishing and mounting to a flat material, the following procedure, demonstrated in Figure 8, was used in fabricating the MEMS phase shifters. Gold transmission lines were electron beam evaporated and patterned using hard contact optical lithography. A silicon nitride (Si_3N_4) layer was deposited using low-temperature Plasma Enhanced Chemical Vapor Deposition (PECVD). The silicon nitride was then patterned and etched using a Reactive Ion Etch (RIE) process everywhere except for the MEMS switch contact areas. Photoresist was patterned to provide a sacrificial layer for the switches. Gold for the switch membrane was evaporated, patterned, electroplated to 2 μm , and etched. The sacrificial layer was stripped away leaving the MEMS switches suspended above the signal lines. The sample was dried using carbon dioxide (CO_2) at the supercritical point to prevent switch collapse due to water surface tension.

IV. PACKAGED MULTIBIT MEMS PHASE SHIFTER

For the first time, RF MEMS phase shifters have been demonstrated on a flexible, organic substrate; specifically, LCP. In addition, this is the first time that a small size four-bit phase shifter was packaged in an organic material. Several modifications were made to the traditional microstrip switched-line phase shifter layout to reduce the size and improve the performance. A four-bit switched-line microstrip phase shifter was designed at 14 GHz for phase shifts between 0° and 337.5° in 22.5° increments, providing a total of 16 different paths (16 cases) [3].

A. Phase Shifter Design

Traditional microstrip theory was used to design the phase shifter. A layout of the final four-bit phase shifter is shown in Figure 9 [3].

The phase shift is related to the change in length between the reference and the phased path. This is described mathematically by Equation 1 where $\Delta\Phi$ is the phase difference (deg), λ is the wavelength, and l is the line length [4].

$$\Delta\Phi = \frac{360}{\lambda} (l_{\text{phased path}} - l_{\text{reference path}}) \quad (1)$$

By routing the signal through different phased path (using MEMS switches), a net phase shift can be achieved.

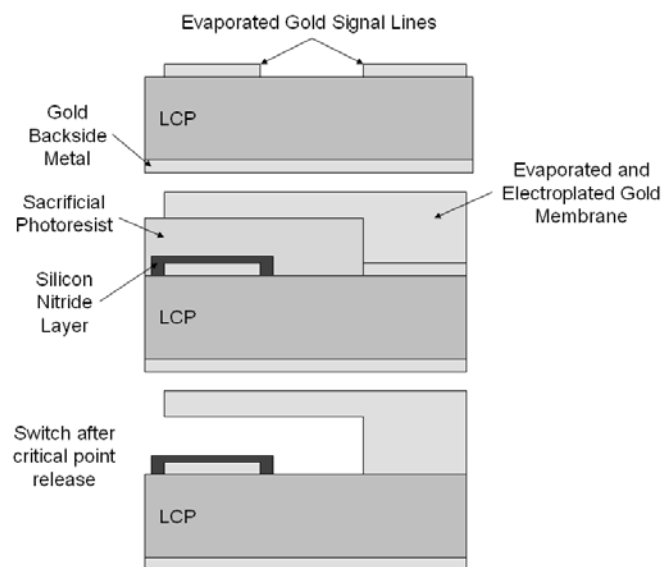


Fig. 8. MEMS switch fabrication process steps.

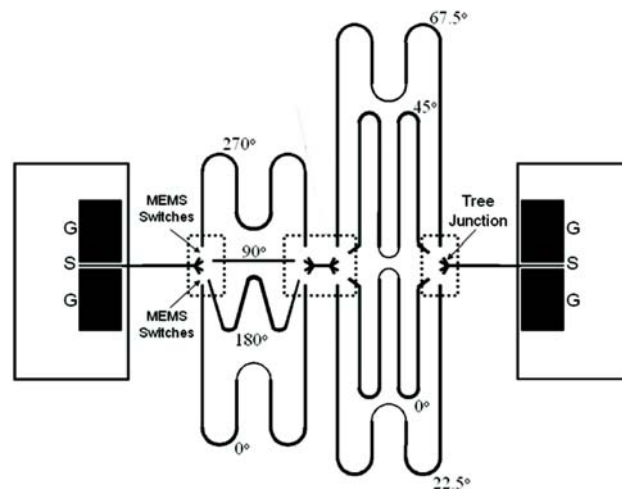


Fig. 9. Top view of the 4-bit series-shunt RF-MEMS phase shifter.

B. Reduced-size Methodology

Switched-line phase shifters are widely used because they are straight-forward to design, fabricate, and integrate with other microwave devices. Unfortunately, the overall size of the switched-line geometry is comparable to the wavelength for each bit. Since multibit phase shifters are usually desired, this can result in a phase shifter that is much larger than the other microwave components in an RF system. For this reason, a number of changes were made to the traditional layout presented in [3] to decrease the size and reduce the loss. These design changes are:

- **Series-shunt implementation:** Instead of cascading four 1-bit phase shifters, which is typically done, we cascaded two 2-bit phaser shifters.
- **High-impedance lines:** Since 50 ohm microstrip lines on LCP have a wide signal width, this limits

the density of the circuit due to significant coupling between lines. Instead, 100 ohm lines were used which decreased the signal width by a factor of 3.7.

- **Curled approach:** The signal lines were curled inward to occupy as less space as possible. If the signal lines were brought together any closer, significant cross coupling would occur.
- **Embedded matching:** Instead of adding stubs or other tuning elements to compensate for the parasitic impedance generated from the curled signal lines, the width of the signal lines were varied to do the matching.

By incorporating these layout changes, the overall area was reduced by a factor of 2.8. The length was reduced by a factor of four. In addition to the size reduction, the signal line length and number of MEMS switches traversed compared to a traditional implementation were each reduced by a factor of two. This results in half the line loss and half the switch loss by using this implementation. A size comparison of the modified layout compared to a traditional layout is shown in Figure 10.

C. Phase Shifter Operation

In order to apply the necessary bias voltage to actuate the MEMS switches, bias pads were designed and placed on each of the signal paths (not shown in Figure 9). When a DC voltage is applied to the bias pad, electrostatic force pulls the switches (which are DC grounded) towards the signal line. A layer of silicon nitride deposited over the signal line prevents switch metal to signal line metal contact. Therefore, no DC current can flow but the capacitance between the switch and the signal line is large enough for RF energy to pass through. The down state capacitance of the MEMS switch is approximately 2.5-4 pF and the up state capacitance is approximately 90 fF. A fabricated four-bit phase shifter with bias pads is shown in Figure 11.

D. Phase Shifter Packaging

As discussed earlier, the presence of the LCP superstrate layer has a negligible effect on the RF performance. The multilayer antennas that were presented in the previous section were bonded using a thermo-compression technique at 300°C. For the LCP package of the phase shifter presented in this paper a commercially available spray epoxy was used to adhere the superstrate layer to the substrate. Cavities were micromachined around the tree-junctions (shown in Figure 11) to prevent the MEMS switches from making contact with the sidewalls. Spray epoxies can be administered easily and cheaply on a large scale, so this method will not significantly increase the cost of production. The degree of hermeticity that the epoxy can provide is still under investigation.

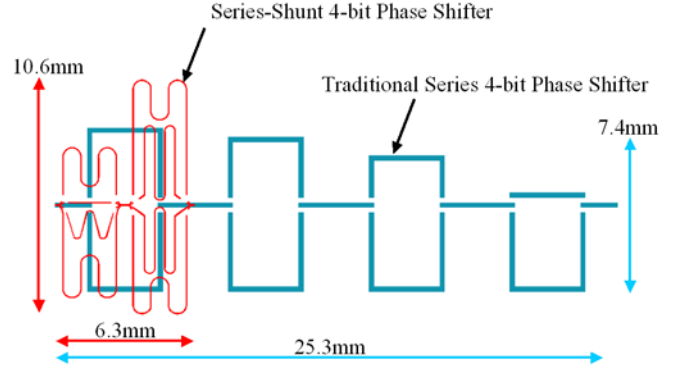


Fig. 10. Size comparison of a 4-bit series-shunt design with traditional series switched-line phase shifter on LCP at 14GHz.

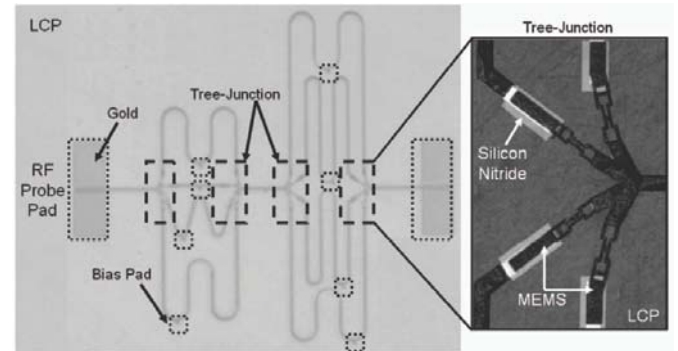


Fig. 11. Picture of the fabricated MEMS phase shifter substrate. The superstrate has been removed and the shown cutouts represent the locations of the cavities and probing windows.

E. Measurements

The loss measurement results for the packaged four-bit MEMS phase shifter are shown in Figure 12. The packaged phase error measurement results are shown in Figure 13. The best case, worst case, and average results are summarized in Table V. The average loss is 0.24 dB/bit, which is the best reported so far for a packaged organic MEMS phase shifter.

Given that the packaged and unpackaged measurement results are almost identical, it can be concluded that the presence of the superstrate layer and the spray epoxy have a negligible effect on the RF performance.

V. ARRAY BEAM SCANNING

Radiometry and radar antenna systems need to be able to scan their radiation pattern over the planet surface to obtain the data required by the NASA ESE. Historically, GaAs MMIC phase shifters are used, but they have high insertion loss, which degrades system sensitivity. In addition, power requirements of GaAs MMICs can be a concern in the design

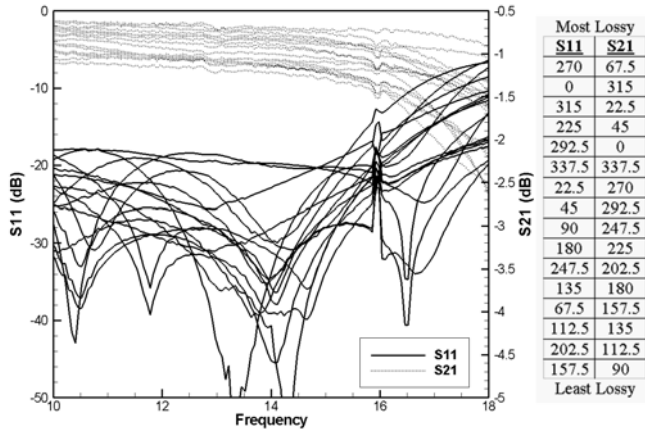


Fig. 12. Measured loss of packaged 4-bit phase shifter. The order of the lines is listed from most lossy to least lossy at 14 GHz.

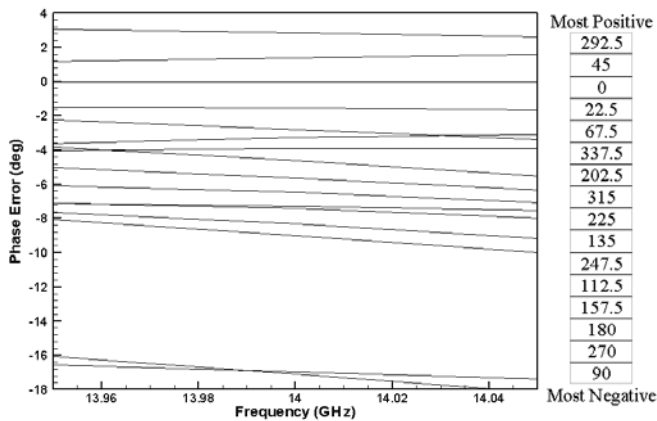


Fig. 13. Measured phase error of packaged 4-bit phase shifter. The order of the lines is listed from most positive to most negative at 14 GHz.

TABLE V
MEASUREMENTS FOR OPEN (UNPACKAGED) AND EPOXY-BONDED (PACKAGED) CONFIGURATIONS OF THE PHASE SHIFTER

	Worst Case	Average	Best Case
Unpackaged S11	-20.8 dB	-30.9 dB	-45.0 dB
Unpackaged S21	-1.22 dB	-0.95 dB	-0.66 dB
Packaged S11	-19.7 dB	-32.5 dB	-45.3 dB
Packaged S21	-1.21 dB	-0.96 dB	-0.69 dB
Unpackaged Phase Error	8.25°	3.96°	0.34°
Packaged Phase Error	17.07°	6.57°	1.38°
S21 Loss Variation	0.045 dB	0.013 dB	0.0022 dB
S21 Phase Variation	9.77°	3.16°	0.27°

of airborne or space borne systems. In this work, MEMS phase-shifters on LCP with low loss and negligible DC power consumption are used. Additionally, RF MEMS routing switches integrated on the same layer with the feed network that can be controlled digitally/electronically via a microprocessor enable the polarization selection (E-pol vs. H-pol). It is anticipated that the 4-bit phase shifter per 2x2 sub-arrays will allow a minimum scanning range of 35 degrees for

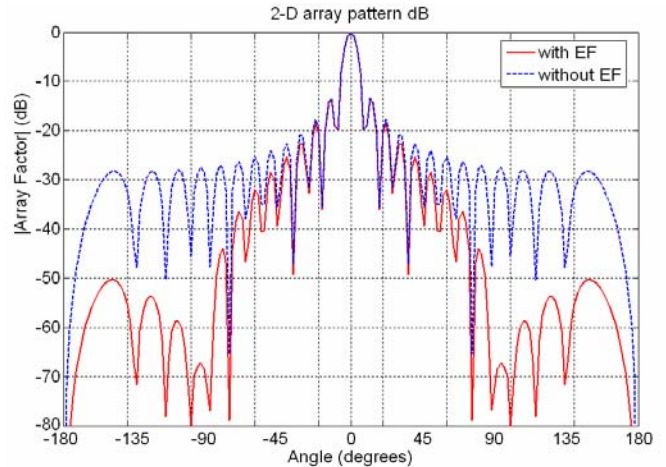


Fig. 14. Effect of the element factor (EF) of microstrip antenna elements on the radiation pattern of the 26x2 array.

the 2x26 antenna array. The array's pattern main cut is shown in Figure 14 for a uniform excitation.

The main lobe has a 3dB beamwidth of 3.5°, which constrains the main beam's steps to those smaller or equal to this angle. This can also define the number of bits needed per phase shifter, which in this case was found to be 4. A larger number of bits would provide smoother beam steering, while a smaller one would provide a more abrupt beam steering, which cannot be used unless a -10dB beamwidth is acceptable. As shown in Figure 15, by using a 4-bit phase-shifter, smooth steps for beam rotation up to an angle of 18 degrees are achieved, without the formation of significant sidelobes. The noticed decrease in the amplitude of the pattern is due to the element factor of the antenna elements that was taken into account.

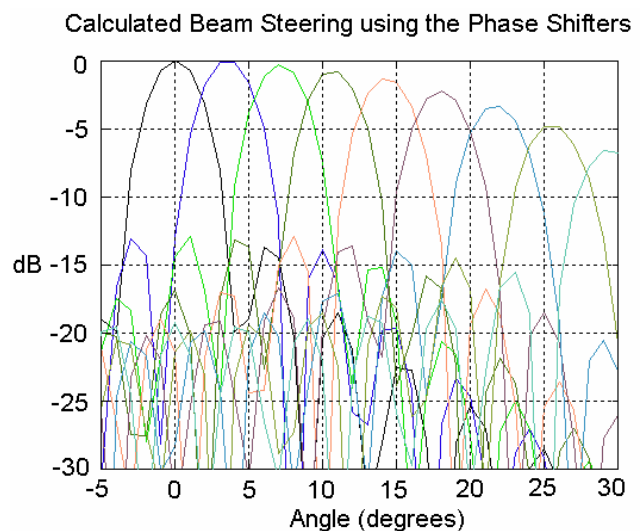


Fig. 15. Beam-steering capability of the 26x2 array, using one phase-shifter every each 2x2 sub-array.

VI. CONCLUSIONS

A dual-frequency, dual-polarization microstrip antenna array for SOP RF front ends was presented for the first time on a flexible multilayer substrate. The design was simulated using commercial full-wave simulation software. The array was fabricated and the measured performance with respect to its scattering parameters and radiation patterns was analyzed. The measurements showed return loss of better than -20 dB, with good cross-polarization characteristics. These designs can be extended to arrays of larger dimensions. In addition, a packaged 4-bit MEMS phase shifter at 14 GHz was also demonstrated on the flexible substrate. With an average per-bit insertion loss of only 0.24 dB, this is one of the lowest loss phase shifters ever documented. The method used to reduce the size of the phase shifter at 14 GHz could also be applied to a design at 35 GHz (as well as any other frequency). Additionally, the multibit phase-shifter can be easily integrated with an antenna array to enable beam steering, which is necessary for remote sensing of precipitation. The results shown here pave the way for the development of low cost, lightweight, and low power RF front ends and antennas on an “all-package” solution for future communication and remote sensing systems.

REFERENCES

- [1] D.M. Pozar and T.A. Metzler, “Analysis of a reflectarray antenna using microstrip patches of variable size,” *Electronics Letters*, pp. 657-658, Apr. 1993.
- [2] J. Huang and A. Fera, “Inflatable microstrip reflectarray antennas at X and Ka-band frequencies,” *IEEE AP-S Symposium*, Vol. 3, pp. 1670-1673, June 1999.
- [3] N. Kingsley and J. Papapolymerou, “Organic ‘Wafer-Scale’ Packaged Miniature Four-Bit RF MEMS Phase Shifter”, *IEEE Transactions on Microwave Theory and Technique*, Vol. 54, No. 3, March 2006.
- [4] Pozar, D., “*Microwave Engineering*, Second Edition”, John Wiley and Sons, Inc, New York, 2001.